Journal of Nuclear Medicine, published on December 4, 2020 as doi:10.2967/jnumed.119.239558

The navigating and de-risking role of ^{89}Zr-immuno-PET in the development of biopharmaceuticals

Guus A.M.S. van Dongen, Wissam Beaino, Albert D. Windhorst, Gerben J.C. Zwezerijnen, Daniela E. Oprea-Lager, N. Harry Hendrikse, Cornelis C. van Kuijk, Ronald Boellaard, Marc C. Huisman, Danielle J. Vugts

Amsterdam University Medical Centers, Vrije Universiteit Amsterdam, Department of Radiology & Nuclear Medicine, Amsterdam, The Netherlands

First/corresponding author

Guus van Dongen

De Boelelaan 1117, 1081 HV Amsterdam, The Netherlands

Phone:+31204442869

Email: gams.vandongen@amsterdamumc.nl

Running title: ^{89}Zr-PET in biological drug development

Keywords: ^{89}Zr-immuno-PET, monoclonal antibodies, biopharmaceuticals, antibody-drug conjugates, immune checkpoint inhibitors

ABSTRACT

The identification of molecular drivers of disease and the compelling rise of biotherapeutics such as peptides, monoclonal antibodies, antibody fragments and non-traditional binding scaffolds, activatable antibodies, bispecific antibodies, immunocytokines, antibody drug conjugates, enzymes, polynucleotides, therapeutic cells as well as alternative drug carriers like nanoparticles have impacted clinical care but also came with challenges. Drug development is expensive, attrition rates are high, and efficacy rates are lower than desired. Nowadays almost all these drugs, that in general have a long residence time in the body, can be stably labeled with ^{89}Zr for whole body-PET imaging and quantification. Although not restricted to monoclonal antibodies, this approach is called ^{89}Zr-immuno-PET. This review summarizes at a high level the State of the Art of the technical aspects of ^{89}Zr-immuno-PET, and illustrates why it has potential for steering the design, development and application of biological drugs. Appealing showcases are discussed to illustrate what can be learned with this emerging technology during preclinical and especially clinical studies about biological drug formats and disease targets. In addition, an overview of ongoing and completed clinical trials is provided. Although ^{89}Zr-immuno-PET is a young tool in drug development, its application is rapidly expanding, with first clinical experiences giving insight why certain drug-target combinations might have better perspectives than others.

INTRODUCTION

Trends and Challenges in Drug Development

The accomplishment of the Human Genome Project in 2003 has boosted the identification of disease targets, the development of targeted drugs, as well as introduction of the concept of personalized therapy. Nevertheless, it is fair to state that new drug development remains challenging with respect to the number of approvals, quality of innovation and cost-effectiveness. About 10 years ago, 20-30 new molecular entities were approved each year. At that time, Research and Development (R&D) productivity defined as the relationship between the value (medical or commercial) created by new medicines and the investment required to generate those medicines, was considered to be the critical factor to be improved, as advocated by Paul et al. in 2010 ***(1)***. They identified the following productivity limiting steps: (i) Drug development is expensive; the average costs to bring a single drug to the market was estimated to be near $ 1 billion; (ii) R&D is inefficient and long-lasting: only 8% of clinical candidate drugs make it to approval, while this process takes more than 10 years. Attrition rates are highest for drugs in early phase clinical trials, while costs are highest when drugs fail in late-stage clinical trials.

Next to R&D efficiency, also the R&D effectiveness, being the distinguished clinical value of a drug, is an important factor in R&D productivity. Also here a lot is desired, taking into account that even registered drugs are only effective in a portion of patients. To reduce phase II and III attrition, Paul et al. proposed two key approaches. First is to have better target selection, i.e. the selection of more validated and druggable targets. Second is the employment of biomarkers, especially in phase I, that assure target engagement or predict and evaluate efficacy and toxicity.

The Emerging Role of Biologicals

The number of drug approvals has increased from 30 per year on average for the period 2000-2013 to about 50 in the period after ***(2)***. One of the reasons was the raise of biologicals, monoclonal antibodies (mAbs) in particular. In the period 2010-2013 the share of biologicals was about 25% of the new US Food and Drug Administration (FDA) approved drugs, during the period 2014–2018 this was 47% ***(3)***. These comprised, hormones, clotting factors, enzymes,

vaccines, nucleic acid products, engineered cell-based products and especially mAbs (50% share). With 570 antibodies at various clinical stages in 2019, including 62 in late-stage clinical studies, continuation of these trends can be expected for the coming years ***(4)***. In 2018, the share of biologicals was $ 251 billion of the world-wide drug market valued at about $ 1000 billion/year, and it is expected to reach $ 625 billion in 2026. Despite these dizzying numbers, the success rate to reach drug approval remained almost constant at around 10%. These are overall figures, and it should be realized that drug development in certain disease areas like mental/brain diseases is even less successful, confirming the difficulty of R&D in these areas ***(5)***.

Potential Role of ^{89}Zr-Immuno-PET

Motivated by aforementioned trends, ^{89}Zr-immuno-PET was developed by our group for PET imaging of mAbs and clinically applied for the first time in 2006 ***(6)***. At that time, the majority of approved mAbs were conventional immunoglobulin G (IgG) molecules, mostly used as antagonists for selective inhibition of receptor tyrosine kinases or to modulate/block other critical membrane targets in cancer and other diseases. The safety and therapeutic success of this first-generation mAbs has stimulated the development of next-generation mAb constructs, which have increased potency, multiple binding domains, or bind to novel targets such as immune checkpoints. Among others, these constructs comprise antibody-drug conjugates (ADCs), bi-specific mAbs that recognize 2 different targets, fusion mAbs like immunocytokines and mAb fragments. Introduction of all these smart targeted molecules is accompanied by questions about their behavior and biodistribution in the human body. Nowadays, the term immuno-PET is also used for tracking of other slow kinetic targeting vehicles such as therapeutic cells (e.g. stem cells and immune cells) and nanoparticles.

The past decade, ^{89}Zr-immuno-PET has been recognized by academic as well as pharma research centers as a powerful tool in drug development and precision medicine, both preclinically and clinically, for a variety of *in vivo* purposes: (i) assessment of target expression, (ii) evaluation of the behavior of the drug in relation to its intrinsic properties, and optimization of drug design, (iii) optimization of dose, route and schedule of administration, (iv) prediction of efficacy and toxicity of drug treatment by performing target occupancy studies, and (v) selection of patients with the highest chance of benefit from drug treatment ***(7)***.

In this review, after summarizing the most important technical aspects of ^{89}Zr-immuno-PET, appealing showcases will be discussed to illustrate the current potential of ^{89}Zr-immuno-PET in the characterization of novel therapeutic biological drugs and their targets. The review is not intending to be comprehensive with respect to PET imaging in drug development, for this we refer to other reviews ***(8-10)***.

TECHNICAL STATE OF THE ART ^{89}ZR-IMMUNO-PET

^{89}Zr-Labeled Tracer Production

To enable the visualization and quantification of a targeted drug with a PET camera, the drug should be labeled in an inert way with a positron emitting radionuclide. Moreover, the physical half-life of the positron emitter should be compatible with the residence time of the drug in the body, which is typically several days to weeks for long-circulating intact mAbs of 150 kDa. This makes the positron emitter ^{89}Zr with its half-life of 78.4 h a preferred isotope, also with regard to ease of transportation/logistics. In addition, ^{89}Zr is a residualizing isotope that becomes trapped inside the cell after internalization by the mAb, while its physical characteristics are very well suited for high resolution and quantitative PET imaging.

^{89}Zr can be produced efficient by irradiation of natural yttrium with 13 MeV protons (^{89}Y(p,n)^{89}Zr nuclear reaction). Nowadays, several academic and commercial suppliers make ^{89}Zr available worldwide on a daily base.

For stable coupling of ^{89}Zr to targeting ligands like mAbs, a chelator has to be used. Currently, the majority of ^{89}Zr-immuno-PET studies employ desferrioxamine B (DFO). The most often employed conjugation procedures make use of either the 2,3,5,6-tetrafluorophenol (TFP) activated ester of *N*-succinyl-DFO-Fe (TFP-*N*-suc-DFO-Fe in which DFO is protected by Fe^{3+}) or p-isothiocyanatobenzyl-DFO (DFO-Bz-NCS), forming respectively stable amide or thiourea bonds with lysine residues in proteins. Both chelators are commercially available and for both detailed conjugation and labeling protocols for the current Good Manufacturing Practice (cGMP)-compliant production of ^{89}Zr-labeled mAbs have been published ***(11-12)***. While radiolabeling is mostly performed manually, procedures for fully automated cGMP-compliant production of ^{89}Zr-labeled mAbs on a commercially available synthesis module have been described ***(13)***. Although several modifications of aforementioned protocols have been proposed to extend the applicability of ^{89}Zr-immuno-PET, e.g. by providing various options for random as well as site-specific conjugation, the basic principles have not been changed over the years ***(14,15)***. Nevertheless, it appeared from preclinical studies that the ^{89}Zr-DFO complex is prone to dissociation *in vivo*, resulting in free ^{89}Zr which accumulates in bone tissue. Many efforts have been invested to develop chelators with increased *in vivo* stability. From an inorganic chemistry

perspective, DFO is not the ideal coordinating molecule for ^{89}Zr, because DFO is a hexadentate chelator consisting of three hydroxamate moieties while Zr^{4+} prefers forming octadentate complexes. With this in mind, at least 15 new chelators have been proposed recently ***(14,16)***. When comparing the performance of these chelators it appears that the octadentate analogue of DFO consisting of four hydroxamate moieties, called DFO* ("DFO star"), is able to solve the instability issues as observed with ^{89}Zr-DFO ***(17)*****(Figure 1)**. Since the bifunctional variant DFO*-NCS is now commercially available, its translation to the clinic can be expected soon.

Several papers describe the quality controls that are needed for the manufacturing of ^{89}Zr-labeled products according to cGMP for clinical use ***(11,12)***. By following such an approach, the extrapolation can be made that the properties of the ^{89}Zr-labeled drug do not deviate from those of the parental drug. Since extensive data revealed the clinical safety of the DFO-based chelators, it can be justified that toxicology studies performed with the parental drug (for human use) are sufficient to allow also the clinical use of the ^{89}Zr-labeled drug. Regulatory agencies of several European countries as well as of the USA have adopted this policy, which eases the integration of ^{89}Zr-immuno-PET into clinical research.

^{89}Zr-Tracer Quantification

PET has the intrinsic potential to quantify the uptake of ^{89}Zr-labeled drugs in diseased areas and normal organs. Makris et al. have addressed the accuracy of quantification by providing ^{89}Zr scanning procedures, which independently of the scanner type/vendor results in harmonized image quality ***(18)***. For this purpose, next to scanner cross-calibration also image noise and recovery coefficients have to be aligned. Standardization of the quantification of ^{89}Zr-labeled compounds will enhance the potential impact of immuno-PET and facilitate evaluation in multicenter trials.

Drug uptake can be expressed as Standard Uptake Value (SUV) or percentage injected dose per gram of tissue (%ID/g). While it might seem attractive to relate mAb uptake with for example target antigen expression, efficacy and toxicity, it is important to realize that total tissue uptake is the sum of "target-specific contribution" (i.e. specific uptake) and non-specific uptake. Non-specific uptake can be reversible (e.g. blood volume) or irreversible (due to ^{89}Zr-residualization after mAb uptake and degradation by antigen-negative cells). Jauw et al. recently described the non-specific uptake of mAbs in normal tissues without known target expression by

using quantitative ^{89}Zr-immuno-PET at multiple time points ***(19)***. These results form a crucial basis for determination of target-occupancy, i.e. the target-specific drug uptake. While the non-specific contribution might be relatively constant for normal tissues across patients, this most probably will not be the case for tumors and therefore more sophisticated modelling strategies have to be developed.

The level of target-specific mAb uptake as measured with ^{89}Zr-immuno-PET might depend on the mAb dose used and can lead to erroneous interpretations with respect to the tumor-targeting potential of the drug. When the mAb dose is too high, target saturation might occur, resulting in low tumor-to-nontumor ratios and poor delineation of tumors on PET images. However, poor tumor-targeting on PET might also be the result of a mAb dose that is too low, for instance when there is a high level of target antigen expression in well-accessible normal organs ("antigen sink") or when there is soluble (shed) target antigen present in the blood circulation. Since tumor target engagement and the identification of potential "antigen sinks" are informative in the *in vivo* characterization of novel candidate mAb-target combinations, it is recommended to apply ^{89}Zr-immuno-PET (pharmacokinetics included) in mAb dose escalation studies.

Also technical advancements like the introduction of total-body PET/CT scanners, having unprecedented sensitivity and high spatial resolution, will likely facilitate assessment of target engagement. As shown recently, the combination of total-body PET and highly stable DFO* chelators enables meaningful ^{89}Zr-antibody-PET studies up to 30 days post-injection ***(20)***. At such late time points it can be anticipated that ^{89}Zr tissue uptake is dominated by the target-specific contribution, while blood pool contribution will be negligible. However, wide introduction of total body PET/CT systems may be hampered by their high costs and availability. Therefore, good yet less optimal alternatives are the recently introduced digital PET/CT systems with an axial field-of-view of ~20 cm or more. These digital systems have excellent sensitivities and improved time-of-flight performance compared with current analogue systems and these systems already show improved image quality and/or provide opportunities to lower injected activities thereby reducing radiation burden ***(21)***. Most studies with intact mAbs use 37-74 MBq ^{89}Zr and result in an effective radiation dose of 20-40 mSv ***(22)***. This is justified for cancer patients, but not for non-oncological patients for whom the dose limit in Europe is 10 mSv. Since total body PET/CT is 20-40 times and digital systems about 3 times more sensitive for total body imaging than conventional PET/CT, this opens opportunities for using less radioactivity, late

imaging time points, repeated tracer administration, imaging in diseased as well as healthy subjects, adults and children, and combinations of these.

^{89}ZR-IMMUNO-PET IN DRUG DEVELOPMENT

^{89}Zr-immuno-PET can be used for the *in vivo* validation of targeting compounds and disease targets. To this end, the *in vivo* biodistribution of biological drugs, including target occupancy, can be studied in relation to: (1) drug characteristics such as specificity, affinity, size, dose, functional modifications and physico-chemical properties in general, (2) target/antigen expression, modulation and internalization, and (3) route of administration. Based on the biodistribution findings, strategies can be explored to further improve target engagement, drug delivery and drug potency with the aim to widen the therapeutic window. In the next section some appealing examples will be discussed where ^{89}Zr-immuno-PET is used to characterize key features of biologicals.

Monoclonal Antibodies

Most of the ^{89}Zr-immuno-PET studies have been performed with conventional FDA-approved intact mAbs, directed against well-characterized antigens expressed on cancer lesions. Therefore these studies are focusing on response prediction and patient selection rather than on drug and/or target selection ***(23)***. Next to these approved mAbs, more recently several other ^{89}Zr-labeled biopharmaceuticals entered clinical trials as comprehensively shown by **Supplemental Table 1** including related publications ***(1-56)***.

Trastuzumab, directed against human epidermal growth factor receptor-2 (HER2), has been most intensively studied ***(23)***. In a first clinical study, ^{89}Zr-immuno-PET was applied in 14 patients for imaging of HER2-positive metastatic breast cancer lesions ***(24)***. ^{89}Zr-trastuzumab was used at dose of 10 or 50 mg for those patients who were trastuzumab-naïve and of 10 mg for those who were already on trastuzumab treatment. **Figure 2** clearly illustrates the dose-dependent biodistribution of ^{89}Zr-trastuzumab. The 10 mg trastuzumab dose resulted in a relatively high uptake in the liver and a pronounced intestinal excretion of ^{89}Zr-trastuzumab, which can be explained by low levels of circulating HER2 in the blood (antigen sink) causing complex formation and excretion via the liver. However, with the 50 mg dose, ^{89}Zr-immuno-PET revealed uptake of trastuzumab in most of the known lesions, brain metastases included, and previously

undetected lesions **(Figure 3)**. No evidence for HER2 expression in normal organs was found, which was confirmed by quantitative PET analysis ***(19)***. These results indicate that the drug-target combination trastuzumab-HER2 shows ideal properties for selective tumor targeting, and therefore justifies the development of more potent anti-HER2 therapeutics.

Targeting of HER2 is more tumor-selective than targeting of the ErbB receptor family members HER1 (i.e. EGFR, epidermal growth factor receptor) and HER3, as revealed from clinical trials with ^{89}Zr-labeled cetuximab (anti-EGFR) and the mAbs RG7116 (lumretuzumab) and GSK2849330, both directed against HER3 ***(25-27)***. With ^{89}Zr-cetuximab besides tumor-targeting also increased liver uptake (up to 23 %ID) was observed during the first days after injection ***(25)*** **(Figure 4)**. While ^{89}Zr-immuno-PET images always show liver uptake due to normal mAb catabolism, in case of ^{89}Zr-cetuximab the liver uptake appeared much higher and can be explained by physiological EGFR expression ***(19)***. Increased liver and spleen uptake was also observed with the two mentioned anti-HER3 mAbs ***(26,27)***. These results indicate that normal tissue expression of EGFR and HER3 hampers efficient tumor targeting, and might limit the employment of potent drug formats directed against these targets.

Immune Checkpoint Inhibitors

Next to tumor cells also stromal cells like immune cells or fibroblasts are exploited as target cells for therapy with biologicals. Immune checkpoint inhibitors (ICIs), which can block immune inhibitory checkpoints and, by doing so, boost T-cell mediated anti-tumor response, have been proven to be particularly successful. Therapy with approved mAbs targeting cytotoxic T-lymphocyte-associated antigen 4 (anti-CTLA-4 ipilimumab), programmed cell death protein 1 (anti-PD-1 nivolumab, pembrolizumab and cemiplimab) and programmed death ligand 1 (anti-PD-L1 atezolizumab, avelumab and durvalumab) results in durable responses in various tumor types. The list of biologicals, targets and indications for ICI therapy is steadily growing. Despite this progress, just a small portion of eligible patients respond to ICI therapy, and this raises the question: why? ***(28)***. These exciting developments have boosted the exploration of imaging biomarkers for ICI therapy ***(29)***. Although clinical imaging of ICIs is at a very early stage, two trials have been reported. In one study, PET with ^{89}Zr-atezolizumab (PD-L1) was performed in 22 patients prior to atezolizumab treatment ***(30)***. Tumor uptake of ^{89}Zr-atezolizumab positively correlated with response to atezolizumab treatment where immunohistochemistry failed to predict

treatment response. In addition, high uptake of ^{89}Zr-atezolizumab was found in healthy lymphoid tissues, including spleen, lymph node and Waldeyer's ring, raising the question whether such uptake might be responsible for immune-related adverse events. In another study, ^{89}Zr-nivolumab (PD-1) and an ^{18}F-labeled anti-PD-L1 adnectin protein (^{18}F-BMS-986192) were both evaluated in 13 non-small cell lung cancer patients prior to nivolumab treatment ***(31)***. It is assumed that high PD-L1 expression by tumor cells together with high PD-1 expression by tumor infiltrating lymphocytes, is a favorable condition for response to anti-PD1/PD-L1 ICI therapy. In this study, tumor uptake of both tracers correlated with PD1 and PD-L1 expression as assessed by immunohistochemistry in tumor tissue, as illustrated by **Figure 5**. For both tracers, a higher tumor uptake was found in responding tumors compared to non-responding tumors, however, this predictive value needs to be confirmed in larger patient cohorts.

Antibody Drug Conjugates (ADCs)

ADCs are "Trojan horses" of antibody development: they represent a targeted approach to treat cancer allowing the selective delivery of therapeutic drugs ("payloads") to the malignant cells by mAbs, thus avoiding damaging of healthy cells. Currently, nine ADCs are approved by the FDA and >100 ADCs are under clinical evaluation ***(32)***. ADCs comprise three components: a disease-selective mAb, a highly potent small-molecule therapeutic payload, and a linker that connects the two parts. Ideally, the ADC is fully stable in the circulation and selectively accumulates to a high extent and homogeneously in the tumor, where it is internalized and the drug is released to exerts its toxic effects. Despite the growing interest, several ADCs failed very recently, mostly due to insufficient efficacy or unforeseen toxicities ***(32,33)***. Toxicities can be due to the unfavorable selectivity/specificity of the antibody, as has occurred with ADCs based on anti-EGFR antibodies (*vide supra*). Still, it can also be related to the instability of the linker system and/or the poor solubility of the drug used. First, the drug can be released from the mAb in the circulation, resulting in sequestration of the drug in normal tissues. Second, the mAb can be destabilized by drug conjugation, resulting in faster blood clearance of the ADC, and sequestration in catabolic organs such as liver and spleen. Destabilization occurs when the drug-to-mAb ratio (DAR) is too high, especially when the drug is hydrophobic. Third, after uptake of an ADC by the tumor cell and subsequent catabolism, the drug can be detached from the ADC and eventually be released from

the cell, enter the circulation and cause toxicity. Trends and challenges in ADC development have been described in a recent review **(*33*)**.

Several ^{89}Zr-immuno-PET studies have been performed to support the development and application of ADCs. Most of these studies have been performed with the radiolabeled parental antibody and not with the radiolabeled ADC ***(34-38)*.** The use of radiolabeled parental mAb for imaging might be informative to assess the tumor-selectivity and target occupancy, and to predict efficacy of ADC treatment ***(37,38)***. Related to this, it is not surprising that HER2 has been recognized as an ideal target for ADC approaches (*vide supra*). In fact two anti-HER2 ADCs have been FDA approved for treatment of metastatic breast cancer, adotrastuzumab emtansine (Kadcyla®, T-DM1) and trastuzumab deruxtecan (Enhertu®, DS-8201), while several others are under development ***(32)***. Because drug loading might affect the biodistribution of a mAb, ^{89}Zr-immuno-PET is most informative when the ADC itself ("carrier + cargo") is radiolabeled rather than just the parental antibody (the "carrier"), as has been explored in some preclinical studies ***(39-43)***.

For the *in vivo* evaluation of ADCs it is important to learn from both, the biodistribution of the mAb and of the therapeutic payload. Cohen et al. used dual radiolabeling by covalently coupling ^{131}I-labeled tubulysin analogues as therapeutic payload to ^{89}Zr-labeled trastuzumab resulting in ^{131}I-TUB-^{89}Zr-trastuzumab ADCs ***(41)***. By doing so, the stability of the ADCs could easily be demonstrated *in intro* as well as *in vivo*. Moreover, it could be concluded that coupling of the tubulysin analogues did not alter the pharmacokinetics and tumor-targeting properties of trastuzumab (inert coupling).

In their effort to characterize the *in vivo* stability of a novel ADC linker, the platinum-based linker [ethylenediamineplatinum(II)$^{2+}$ (called *Lx*®), Muns et al. labeled the mAb with ^{89}Zr, the *Lx* linker with ^{195m}Pt (^{195m}Pt, gamma emitter with a half-life time of 4.02 days), while ^{89}Zr-DFO was also exploited as an artificial payload ***(42)***. Similar biodistribution was observed irrespective of the isotope measured, which led to the conclusion that *Lx*-based ADCs are fully stable *in vitro* and *in vivo*, and capable of optimal delivery of the artificial payload to tumors. In a next step, the commonly used therapeutic payload auristatin F (AF) was coupled at various molar ratios to trastuzumab via the *Lx* linker followed by ^{89}Zr labeling to obtain ^{89}Zr-DFO-Trastuzumab-*Lx*-AF with AF-to-antibody ratios of 0, 2.6 or 5.2. **(Figure 6)**. While ADCs with a DAR of 2.6 showed the same selective tumor targeting as the parental antibody (indicated as DAR = 0), the ADC with

a DAR of 5.2 showed a dramatically impaired tumor targeting, faster blood clearance, and increased liver uptake. After validation of optimal tumor targeting by imaging, the trastuzumab-*Lx*-AF ADC appeared to outperform FDA-approved ado-trastuzumab emtansine in therapy studies in tumor-bearing mice ***(43)***.

Activatable Antibodies

Unfortunately, only a limited number of target antigens have a high expression on tumor/diseased tissue and a very low expression on healthy tissue. Activatable antibodies, like those under development by CytomX Therapeutics (so-called Probody® therapeutics), represent a potential new approach for improving the selectivity and homogeneity of tumor targeting by antibodies. This approach aims widening of the therapeutic window, and increasing the number of candidate targets that are suitable for targeting with potent antibody constructs like ADCs. Activatable antibodies are recombinant antibody prodrugs in which the antigen-binding domains are "masked" and converted to active antigen-binding antibodies inside the tumor environment by tumor-associated proteases **(Figure 7)**. First *in vivo* proof of concept was obtained with an anti-EGFR Probody® therapeutic based on the anti-EGFR mAb cetuximab ***(44)***. In these studies, it was demonstrated that the Probody remained masked until activated by proteases in the tumor environment, a way to circumvent accumulation of cetuximab in normal tissues (e.g. liver and skin). Two Probody therapeutic candidates have been evaluated in preclinical ^{89}Zr-immuno-PET studies.

In one study, the tumor-targeting performance of the anti-CD166 Probody drug conjugate CX-2009, a Probody therapeutic coupled with the toxic drug DM4, was labeled with ^{89}Zr and evaluated with PET in xenograft bearing mice ***(45)***. CD166 is overexpressed on the outer cell surface of many tumor types but is also present in several healthy organs. In this study, the biodistribution of CX-2009 was compared with the biodistribution of (1) the Probody therapeutic itself (without drug), (2) the parental mAb (no mask), and (3) the parental mAb coupled with DM4 (ADC). These studies demonstrated that CX-2009 is capable of optimally targeting CD166-expressing tumors when compared with its parental compounds, implying that enzymatic activation inside the tumor, required for CD166 binding, does not limit tumor targeting. Reduced targeting of healthy organs cannot be demonstrated in rodents as CX-2009 does not bind to mouse CD166, however, ongoing clinical ^{89}Zr-immuno-PET studies should provide confirmation.

In another preclinical study, it was demonstrated that the anti-PD-L1 Probody CX-072 therapeutic became activated in tumors, resulting in preferential tumor uptake while accumulation in spleen and other PD-L1-expressing peripheral lymphoid organs appeared to be limited ***(46)***. These results indicate that CX-072 may reduce anti-PD-L1-mediated toxicity in healthy tissues. These intriguing findings will be confirmed in ongoing clinical ^{89}Zr-CX-072 studies.

Bispecific Antibodies and Immunocytokines

Currently >90 bispecific antibodies (BsAbs) have been developed, mostly for oncological applications ***(47)***. Since such constructs contain two (or more) antigen-binding regions directed against two different targets, their biodistribution is hard to predict and will depend among others on the expression level and accessibility of each of the targets, and the affinity of each antibody arm for its particular antigen. Appropriate targeting, which means simultaneous binding to both targets, is well possible for hemato-oncological applications like in case of the FDA approved anti-CD3-CD19 BsAb blinatumomab, because here the CD3+ cytotoxic T cells (effector cells) and the CD19+ B cells (target cells) are residing in the same blood compartment. However, appropriate targeting will theoretically be much more challenging in case of solid tumors. For example, an anti-CD3-HER2 BsAb that is administered intravenously will most likely show impaired tumor targeting, since the anti-CD3 arm will cause "stickiness" of the BsAb to T cells in the blood compartment. A few clinical ^{89}Zr-immuno-PET studies indicate that the latter indeed seems to be the case.

Moek et al. evaluated a 55 kDa ^{89}Zr-labeled BsAb directed against CD3 and the carcinoembryonic antigen (CEA) in 9 patients with advanced gastrointestinal adenocarcinomas ***(48)***. The tracer was administered either at a low dose of 0.2, 2 or 5 mg BsAb, or during a treatment period in which the patients received 6.4 of 12.8 mg BsAb/day by continuous intravenous administration via a central venous access port. As might have been expected, images with the tracer dose revealed accumulation of ^{89}Zr-labeled anti-CD3-CEA BsAb in CD3-rich lymphoid organs, as well as inter- and intra-individual heterogenous tumor uptake. Interestingly, tracer administration during BsAb treatment revealed the presence of the tracer in the blood pool, whereas tumor lesions were not visualized, possibly reflecting target saturation. These studies indicate that target saturation in the tumor might be possible, although at the expense of using an

inconvenient administration procedure. To improve tumor-targeting and to avoid on-target off-tumor toxicity, several novel BsAb constructs are under development, including BsAbs comprising a masked CD3 arm, which need activation inside the tumor to exert their bispecific activity (vide supra) ***(49)***.

Similar observations have been made with the immunocytokine cergutuztumab amunaleukin (CEA-IL2v), an immunocytokine directed against CEA with abolished IL-2α receptor (IL2Rα) binding, which is designed to cause intra-tumoral IL2-mediated immune potentiation ***(50)***. Next to improved uptake in CEA-positive tumors when compared to CEA-negative tumors, also major accumulation in lymphoid organs was observed compatible with binding to immune cells expressing the IL-2 receptor.

Other Emerging Fields of ^{89}Zr-Immuno-PET

Cell-based therapies, such as adoptive immunotherapy (e.g. chimeric antigen receptor-T cells) and stem cell therapy, have received considerable attention ***(51)***. Also here ^{89}Zr-immuno-PET might be informative to assess the *in vivo* distribution of the therapeutic cell population ***(52)***. Next to identifying (immune) cell subsets with ^{89}Zr-labeled PET tracers based on their specific cell surface markers, adoptive cells can nowadays also be uploaded with ^{89}Zr via ^{89}Zr-oxine, or covalently membrane labeled with ^{89}Zr via DFO, to enable their tracking *in vivo* ***(53)***. For this purpose, cells have to be labeled with sufficient amounts of ^{89}Zr, doing so inertly, i.e. without affecting the cells' biological properties. Although cell tracking with ^{89}Zr-immuno-PET is at a pioneering stage, even the possibility of single-cell tracking by PET has recently been demonstrated in mice ***(54)***.

Next to drug and target characteristics, also the route of administration might be an important variable in the efficient application of biopharmaceuticals, as was illustrated in a couple of ^{89}Zr-immuno-PET studies on brain targeting. One of these studies was the first to apply ^{89}Zr-bevacizumab PET imaging in pediatric patients with diffuse intrinsic pontine glioma, demonstrating low and variable ^{89}Zr-bevacizumab tumor uptake after intravenous administration ***(55)***. These findings indicate the added value of ^{89}Zr-immuno-PET in explaining the very poor prognosis of these patients by blood-brain-barrier (BBB) integrity. Interestingly, in subsequent preclinical PET studies with ^{89}Zr-bevacizumab, Lesniak et al. showed that by intra-arterial

instead of intravenous administration of the conjugate and coadministration of mannitol for opening of the BBB, the brain uptake of ^{89}Zr-bevacizumab became 10-15 times higher ***(56)***. These studies illustrate that ^{89}Zr-immuno-PET could guide delivery of biologicals behind the BBB, with great promise for therapy of brain diseases, neurodegenerative diseases included ***(57)***.

CONCLUSIONS

The field of ^{89}Zr-immuno-PET is expanding very rapidly as exemplified by the increasing number of publications, the types of applications and biopharmaceuticals under study, and the number of clinical trials. As illustrated in this review, ^{89}Zr-immuno-PET has become an important tool for the *in vivo* characterization of biological drugs and the validation of disease targets. While ^{89}Zr-labeling of biopharmaceuticals seems to be technically matured and can for most drug formats be performed in an inert and pharmaceutically acceptable way, improvements in ^{89}Zr-immuno-PET can be expected the coming years by standardization and harmonization of ^{89}Zr quantification by PET imaging and by the introduction of more sensitive PET scanners. In an era of societal debate about "expensive drugs" and affordability of health care, ^{89}Zr-immuno-PET might become a crucial player in improving the efficiency and effectiveness of drug development and in the further evolution of precision medicine.

Disclosure: Dr. Guus van Dongen has an unpaid position of Chief Scientific Officer (CSO) at LinXis biopharmaceuticals.

NOTEWORTHY POINTS

- ^{89}Zr-immuno-PET has become an important tool for the *in vivo* visualization and quantification of biological drugs and the validation of disease targets.
- High quality ^{89}Zr, suitable chelators for coupling, as well as standardized protocols for cGMP-compliant manufacturing of ^{89}Zr-labeled biopharmaceuticals are available.
- ^{89}Zr-immuno-PET is not only used for imaging of antibodies, but also for other slow kinetic drugs, living therapeutic cells included.
- ^{89}Zr-immuno-PET has been adopted by academia as well as by pharma industry.

REFERENCES

1. Paul SM, Mytelka DS, Dunwiddie CT, et al., How to improve R&D productivity: the pharmaceutical industry's grand challenge. *Nat Rev Drug Discov.* 2010;9:203-214.

2. Baedecker M, Ringel M, Schulze U. 2018 FDA approvals hit all time high – but average value slips again. *Nat Rev Drug Discov.* 2019;18:90.

3. Walsh G. Biopharmaceutical benchmarks 2018. *Nat Biotechnol.* 2018;12:1136-1145.

4. Kaplon H, Reichert JM. Antibodies to watch in 2019. *MAbs.* 2019;11:219-238.

5. Pammolli F, Righetto L, Abrignani S, Pani L, Pelicci PG, Rabosio E. The endless frontier? The recent increase of R&D productivity in pharmaceuticals. *J Transl Med.* 2020;18;162.

6. Börjesson PKE, Jauw YWS, Boellaard R, et al. Performance of immuno-positron emission tomography with zirconium-89-labeled chimeric monoclonal antibody U36 in the detection of lymph node metastases in head and neck cancer patients. *Clin Cancer Res.* 2006;12:2133-2140.

7. Jauw YW, Menke-van der Houven van Oordt CW, Hoekstra OS, et al. Immuno-positron emission tomography with zirconium-89-labeled monoclonal antibodies in oncology : what can we learn from initial clinical trials? *Front Pharmacol.* 2016;7:131.

8. Kelloff GJ, Krohn KA, Larson SM, et al. The progress and promise of molecular imaging probes in oncologic drug development. *Clin Cancer Res.* 2005;11:7967-7985.

9. De Vries EGE, Kist de Ruijter L, Lub-de Hooge MN, Dierckx RA, Elias SC, Oosting SF. Integrating molecular nuclear imaging in clinical research to improve cancer therapy. *Nat Rev Clin Oncol.* 2019;16:241-255.

10. Wei W, Rosenkrans ZT, Liu J, Huang G, Luo Q-Y, Cai W. ImmunoPET: concept, design and applications. *Chem Rev.* 2020;120:3787-3851.

11. Vosjan MJWD, Perk LR, Visser GWM, et al. Conjugation and radiolabeling of monoclonal antibodies with zirconium-89 for PET imaging using the bifunctional chelate *p*-isothiocyanatobenzyl-desferrioxamine. *Nat Protoc.* 2010;5:739-743.

12. Cohen R, Vugts DJ, Stigter-van Walsum M, Visser GWM, Van Dongen GAMS. Inert coupling of IRDye800CW and zirconium-89 to monoclonal antibodies for single- or dual-modal fluorescence and PET imaging. *Nat Protoc.* 2013;8:1010-1018.

13. Poot AJ, Adamzek KWA, Windhorst AD, et al. Fully automated ^{89}Zr labeling and purification of antibodies. *J Nucl Med.* 2019;60:691-695.

14. Heskamp S, Raavé R, Boerman O, Rijpkema M, Goncalves V, Denat F. ^{89}Zr-immuno-positron emission tomography in oncology: state-of-the-art ^{89}Zr radiochemistry. *Bioconjug Chem.* 2017;28:2211-2223.

15. Bhatt NB, Pandya DN, Rideout-Danner S, Gage HD, Marini FC, Waddas TJ. A comprehensively revised strategy that improves the specific activity and long-term stability of clinically relevant ^{89}Zr-immuno-PET agents. *Dalton Trans.* 2018;47:13214-13221.

16. Batt NB, Pandya DN, Wadas TJ. Recent developments in zirconium-89 chelator development. *Molecules.* 2018;23:638.

17. Chomet M, Schreurs M, Bolijn MJ, et al. Head to head comparison of DFO* and DFO chelators: selection of the best candidate for clinical ^{89}Zr-immuno-PET. *Eur J Nucl Med Mol Imaging.* 2020, in press, DOI/10.1007/s00259-020-05200-7.

18. Makris NE, Boellaard R, Visser EP, et al. Multicenter harmonization of ^{89}Zr PET/CT performance. *J Nucl Med.* 2014;55:264-267.

19. Jauw YWS, O'Donoghue JA, Zijlstra JM, et al. ^{89}Zr-immuno-PET: Towards a non-invasive clinical tool to measure target engagement of therapeutic antibodies in vivo. *J Nucl Med.* 2019;60:1825-1832.

20. Berg E, Gill H, Marik J, et al. Total-body PET and highly stable chelators together enable meaningful ^{89}Zr-antibody-PET studies up to 30 days post-injection. *J Nucl Med.* 2020;61:453-460.

21. Van Sluis J, Boellaard R, Somasundaram A, et al. Image quality and semiquantitative measurements on the Biograph Vison PET/CT system: Initial experiences and comparison with the Biograph mCT. *J Nucl Med.* 2020;61:129-135.

22. Borjesson PKE, Jauw YWS, De Bree R, et al. Radiation dosimetry of ^{89}Zr-labeled chimeric monoclonal antibody U36 as used for immuno-PET in head and neck cancer patients. *J Nucl Med.* 2009;50:1828-1836.

23. Yoon J-K, Park B-N, Ryu E-K, An Y-S, Lee S-J. Current perspectives on ^{89}Zr-PET imaging. *Int J Mol Sci.* 2020;21:4309.

24. Dijkers EC, Oude Munnink TH, Kosterink JG, et al. Biodistribition of ^{89}Zr-trastuzumab and PET imaging of HER2-positive lesions in patients with metastatic breast cancer. *Clin Pharmacol Ther.* 2010;87:586-592.

25. Menke-van der Houven van Oordt CW, Gootjes EC, Huisman MC, et al. ^{89}Zr-cetuximab PET imaging in patients with advanced colorectal cancer. *Oncotarget.* 2015;6:30384-30393.

26. Bensch F, Lamberts LE, Smeenk MM, et al. ^{89}Zr-Lumretuzumab PET imaging before and during HER3 antibody lumretuzumab treatment is patients with solid tumors. *Clin Cancer Res.* 2017;23:6128-6137.

27. Menke-van der Houven van Oordt CW, McGeoch A, Bergstrom M, et al. Immuno-PET imaging to assess target engagement: experience from ^{89}Zr-anti-HER3 mAb (GSK2849330) in patients with solid tumors. *J Nucl Med.* 2019;60:902-909.

28. Haslam A, Prasad V. Estimation of the percentage of US patients with cancer who are eligible for and respond to checkpoint inhibitor immunotherapy drugs. *JAMA Netw Open.* 2019;2:e192535.

29. Van de Donk PP, Kist de Ruijter L, Lub-de Hooge MN, et al. Molecular-imaging biomarkers for immune-checkpoint inhibitor therapy. *Theranostics.* 2020;10:1708-1718.

30. Bensch F, Van der Veen EL, Lub-de Hooge MN, et al. ^{89}Zr-atezolizumab imaging as a non-invasive approach to assess clinical response to PD-L1 blockade in cancer. *Nat Med.* 2018;24:1852-1858.

31. Niemeijer AN, Leung D, Huisman MC, et al. Whole body PD-1 and PD-L1 positron emission tomography in patients with non-small-cell lung cancer. *Nat Commun.* 2018;9:4664.

32. Joubert N, Beck A, Dumontet C, Denevault-Sabourin C. Antibody-drug conjugates: The last decade. *Pharmaceuticals.* 2020;13:245.

33. Beck A, Goetsch L, Dumontet C, Corvaïa N. Strategies and challenges for the next generation of antibody-drug conjugates. *Nat Rev Drug Discov.* 2017;16:315-337.

34. Carmon KS, Azhdarinia A. Application of immuno-PET in antibody-drug conjugate development. *Mol Imaging.* 2018;17:1536012118801223.

35. O'Donoghue JA, Danila DC, Pandit-Taskar N, et al. Pharmacokinetics and biodistribution of a [^{89}Zr]Zr-DFO-MSTP2109A anti-STEAP1 antibody in metastatic castration-resistant prostate cancer patients. *Mol Pharm.* 2019;16:3083-3090.

36. Chia P-L, Parakh S, Tsao M-S, et al. Targeting and efficacy of novel mAb806-antibody-drug conjugates in malignant mesothelioma. *Pharmaceuticals.* 2020;13:289.

37. Gebhart G, Lamberts LE, Wimana Z, et al. Molecular imaging as a tool to investigate heterogeneity of advanced HER2-positive breast cancer and to predict patient outcome under trastuzumab emtansine (T-DM1): the ZEPHIR trial. *Ann Oncol.* 2016;27:619-624.

38. Williams S-P, Ogasawara A, Tinianow JN, et al. ImmunoPET helps predicting the efficacy of antibody-drug conjugates targeting TENB2 and STEAP1. *Oncotarget.* 2016;7:25103-25112.

39. Al-Saden N, Lam K, Chan C, Reilly RM. Positron-emission tomography of HER2-positive breast cancer xenografts in mice with ^{89}Zr-labeled trastuzumab-DM1: a comparison with ^{89}Zr-labeled trastuzumab. *Mol Pharm.* 2018;15:3383-3393.

40. Kang L, Jiang D, Ehlerding EB, et al. Noninvasive trafficking of brentuximab vedotin and PET imaging of CD30 in lung cancer murine models. *Mol Pharm.* 2018;15:1627-1634.

41. Cohen R, Vugts DJ, Visser GWM, et al. Development of novel ADCs: conjugation of tubulysin analogues of trastuzumab monitored by dual radiolabeling. *Cancer Res.* 2014;74:5700-5710.

42. Muns JA, Montserrat V, Houthoff H-J et al. In vivo characterization of platinum(II)-based linker technology for the development of antibody-drug conjugates: taking advantage of dual labeling with ^{195m}Pt and ^{89}Zr. *J Nucl Med.* 2018;59:1146-1156.

43. Sijbrandi NJ, Merkul E, Muns JA, et al. A novel platinum(II)-based bifunctional ADC linker benchmarked using ^{89}Zr-desferal and auristatin F conjugated trastuzumab. *Cancer Res.* 2017;77:257-267.

44. Desnoyers LR, Vasiljeva O, Richardson JH, et al. Tumor-specific activation of an EGFR-targeted probody enhances therapeutic index. *Sci Transl Med.* 2013;5:207ra144.

45. Chomet M, Schreurs M, Nguyen M, et al. The tumor targeting performance of anti-CD166 Probody drug conjugate CX-2009 and its parental derivatives as monitored by ^{89}Zr-immuno-PET in xenograft bearing mice. *Theranostics.* 2020;10:5815-5828.

46. Giessen D, Broer LN, Lub-de Hooge M, et al. Probody therapeutic design of ^{89}Zr-CX-072 promotes accumulation in PD-L1 expressing tumors compared to normal murine lymphoid tissue. *Clin. Cancer Res.* 2020;26:3999-4009.

47. Sedykh SE, Prinz VV, Buneva VN, Nevinsky GA. Bispecific antibodies: design, therapy, perspectives. *Drugs Des Devel Ther.* 2018;12:195-208.

48. Moek KL, Waaijer SJH, Kok IC, et al. ^{89}Zr-labeled bispecific T-cell engager AMG 211 PET shows AMG 211 accumulation in CD3-rich tissues and clear, heterogeneous tumor uptake. *Clin Cancer Res.* 2019;25:3517-3527.

49. Geiger M, Stubenrauch K-G, Sam J, et al. Protease-activation using anti-idiotypic masks enables tumor specificity of a folate receptor 1-T cell bispecific antibody. *Nat Commun.* 2020;11:3196.

50. Van Brummelen EMJ, Huisman MC, De Wit-Van der Veen LJ, et al. ^{89}Zr-labeled CEA-targeted IL-2 variant immunocytokine in patients with solid tumors: CEA-mediated tumor accumulation and role of IL-2 receptor binding. *Oncotarget.* 2018;9:24737-24749.

51. Khalil DN, Smith EL, Brentjes RJ, Wolchok JD. The future of cancer treatment: immunomodulation, CARs and combination therapy. *Nat Rev Clin Oncol.* 2016;13:273-290.

52. Kircher MF, Gambhir SS, Grimm J. Noninvase cell-tracking methods. *Nat Rev Clin Oncol.* 2011;8:677-688.

53. Bansal A, Pandey MK, Demirhan YE, et al. Novel ^{89}Zr cell labeling approach for PET-based cell trafficking studies. *EJNMMI Res.* 2015;5:19.

54. Jung, K.O. Kim TJ, Yu JH, et al. Whole-body tracking of single cells via positron emission tomography. *Nat Biomed. Eng.* 2020;10:6024-6034.

55. Jansen MH, Veldhuijzen van Zanten SEM, Van Vuurden DG, et al. Molecular drug imaging: ^{89}Zr-bevacizumab PET in children with diffuse intrinsic pontine glioma. *J Nucl Med.* 2017;58:711–716.

56. Lesniak WG, Chu C, Jablonska A, et al. A distinct advantage to intraarterial delivery of 89Zr-bevacizumab in PET imaging of mice with or without osmotic opening of the blood-brain barrier. *J Nucl Med.* 2019;60:617-622.

57. Veldhuijzen-Van Zanten SEM, De Witt Hamer PC, Van Dongen GAMS. Brain access of monoclonal antibodies as imaged and quantified by ^{89}Zr-antibody PET: Perspectives for treatment of brain diseases. *J Nucl Med.* 2019;60:615-616.

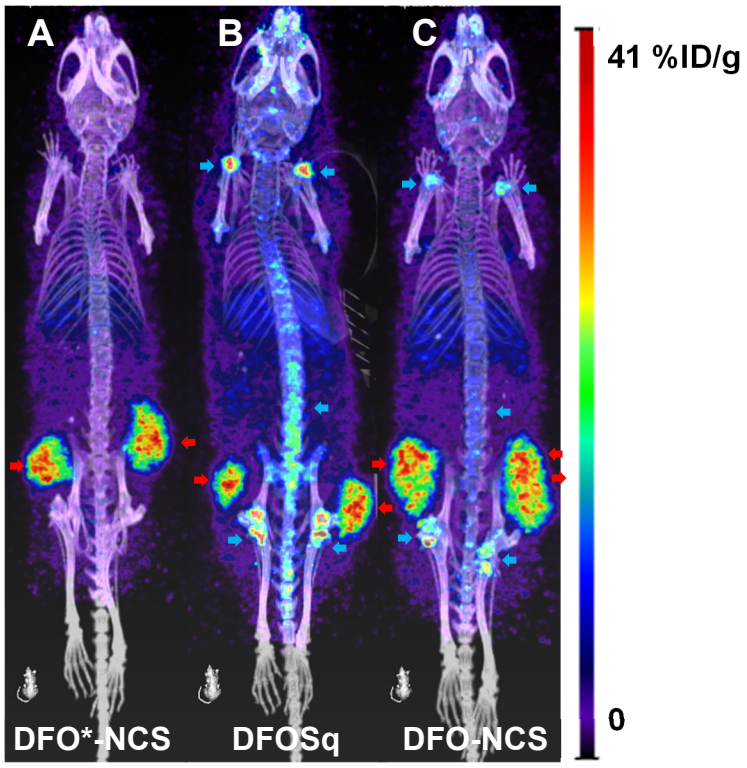

Figure 1: PET images of N87 tumor-bearing mice injected with either [^{89}Zr]Zr-DFO*-NCS-trastuzumab **(A)**, [^{89}Zr]Zr-DFO-Squaramide-trastuzumab **(B)**, or [^{89}Zr]Zr-DFO-NCS-trastuzumab **(C)** and scanned 144 h p.i. Tumors are indicated with red arrows and bone uptake with blue arrows. Note the bone uptake with the two DFO chelators, which is lacking when DFO* is used for ^{89}Zr labeling (*17*).

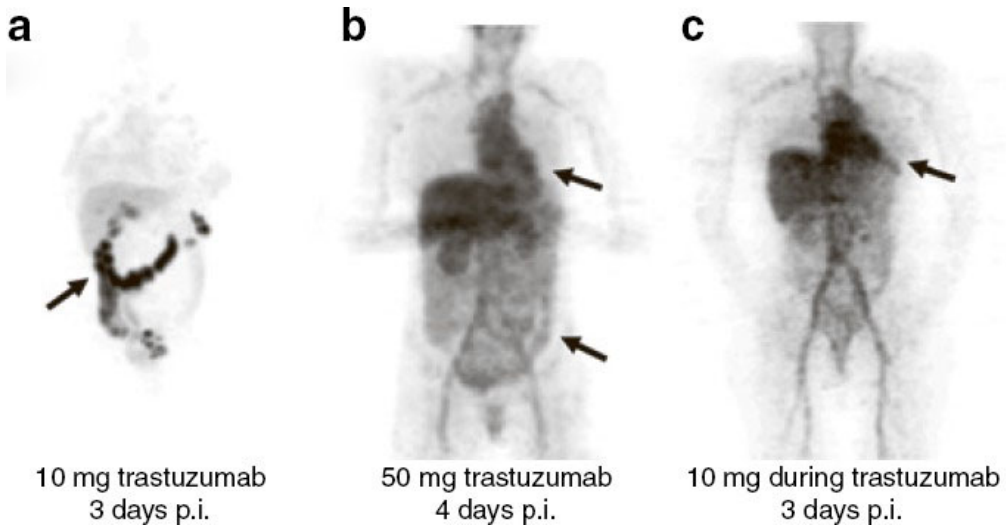

Figure 2. Dose-dependent ^{89}Zr-trastuzumab biodistribution. (**a–c**) Radioactivity in the blood pool and intestinal excretion are indicated by arrows. Note the rapid clearance of trastuzumab from the body at low mAb dose *(24)*.

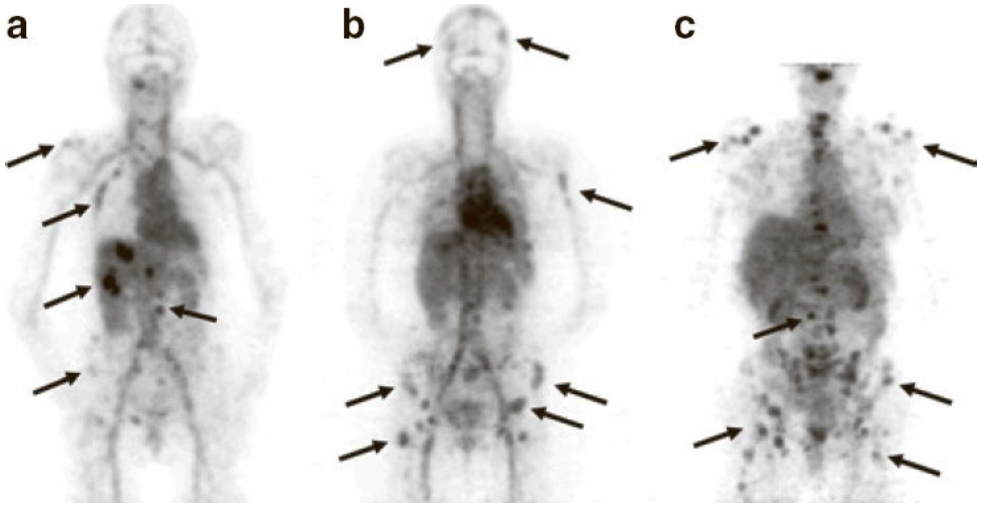

Figure 3. Examples of ^{89}Zr-trastuzumab uptake 5 days after the injection. (**a**) A patient with liver and bone metastases, and (**b** and **c**) two patients with multiple bone metastases. A number of lesions have been specifically indicated by arrows *(24)*.

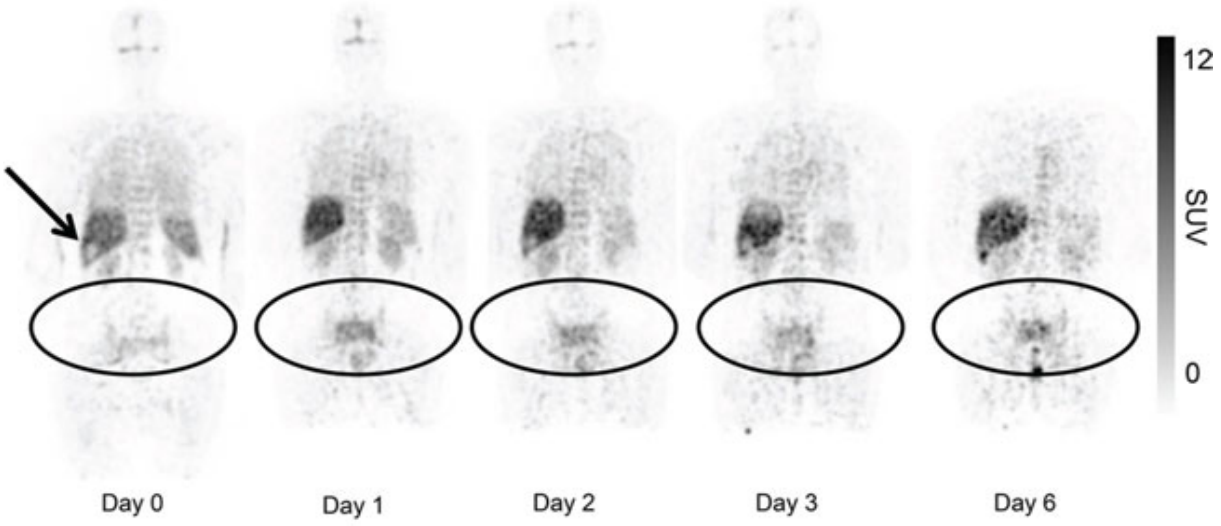

Figure 4: Uptake of ^{89}Zr-cetuximab in a patient with tumor lesions in the pelvis and sacral bone. ^{89}Zr-cetuximab is sequestered in the liver, a relatively photopenic lesion is observed at the site of a liver metastasis (arrow). Accumulation of ^{89}Zr-cetuximab over time is demonstrated in the tumor lesions *(25)*.

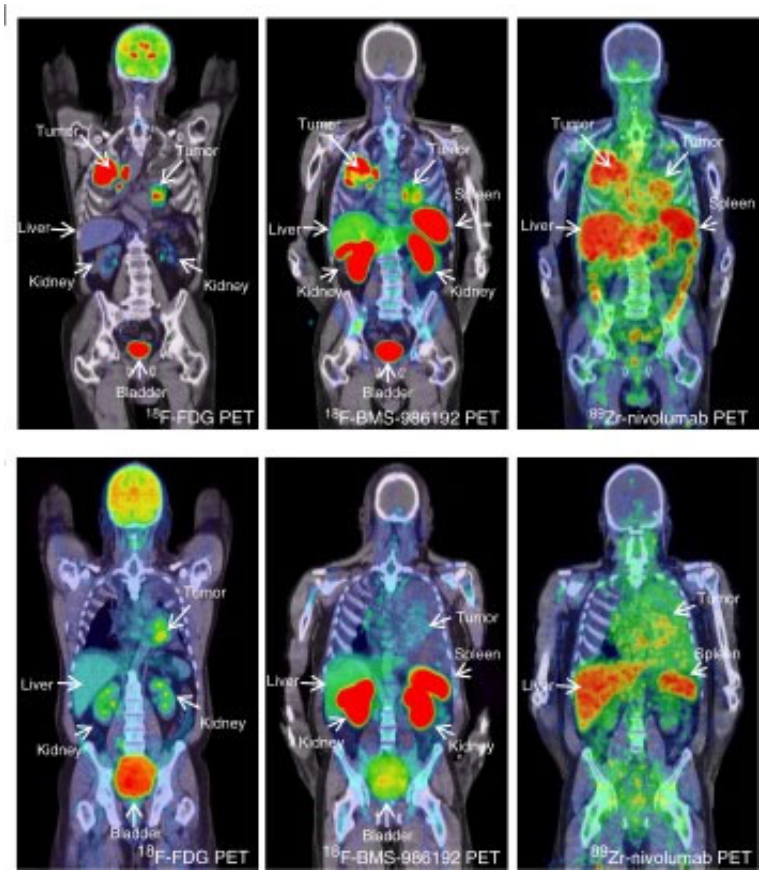

Figure 5. PET-images of two NSCLC patients. Upper row: patient with PD-L1 expression in 95% of the tumor cells. Lower row: Patient with tumor PD-L1 expression < 1%. ^{18}F-FDG PET (left panels) demonstrates high glucose metabolism of tumors in both lungs and mediastinal lymph nodes. ^{18}F-BMS-986192 PD-L1 PET (middle panels) and ^{89}Zr-labeled Nivolumab PD-1 PET (right panels) demonstrate high but heterogeneous tracer uptake in tumors of upper patient and low heterogeneous tracer uptake in the tumor of lower patient *(31)*.

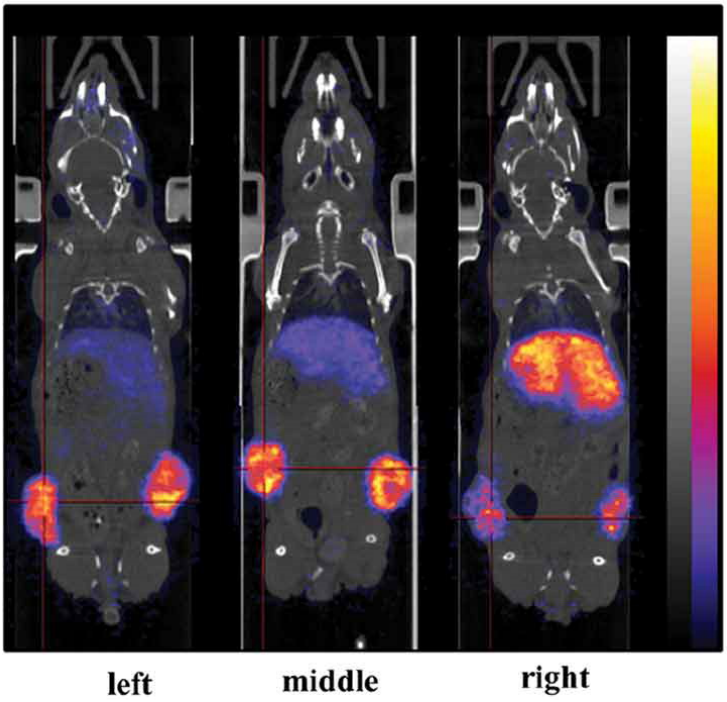

Figure 6. The effect of auristatin F (AF) conjugation via *Lx* linker to trastuzumab on biodistribution characteristics in NCI-N87 bearing nude mice. PET images of ^{89}Zr-trastuzumab-*Lx*-AF with AF-to-mAb ratios of 0 (left panel), 2.6 (middle panel), and 5.2 (right panel) 96 h p.i.. Note impaired tumor targeting and increased liver uptake of the ADC with AF-to-mAb ratio 5.2. *(43)*.

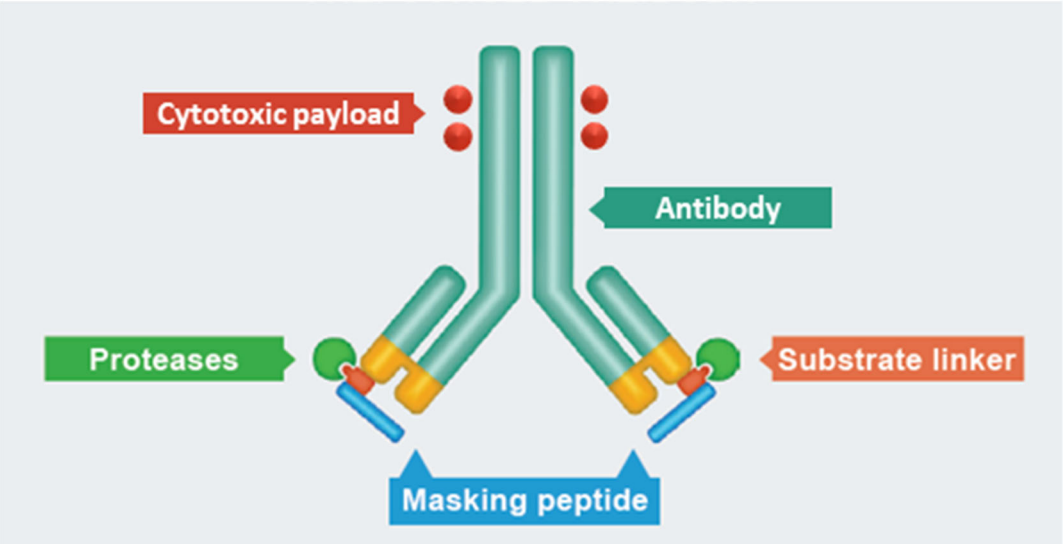

Figure 7: General representation and structure of CX-2009 Probody Drug Conjugate. Reproduced with permission of Cytomx Therapeutics, Inc.

Table 1. ^{89}Zr-labeled biopharmaceuticals in completed or ongoing clinical trials

^{89}Zr-labeled registered biopharmaceutical *	**Target**	**Indication/purpose**	**Trial identified (Year posted)**	**Phase/status**	**References**
Atezolizumab	PD-L1	Locally advanced or metastatic solid tumors	NCT02453984 (2015)	N.A.; recruiting	*(1)*
		Diffuse large-B cell lymphoma	NCT03850028 (2019)	N.A.; recruiting	
		Renal cell carcinoma	NCT04006522 (2019)	Phase 1; recruiting	
		Lobular metastatic breast cancer	NCT04222426 (2020)	N.A.; recruiting	
Avelumab	PD-L1	Non-small cell lung cancer	NCT03514719 (2018)	Phase 1; recruiting	
Bevacizumab	VEGF	Metastatic renal cell carcinoma	NCT00831857 (2009)	N.A.; completed	*(2)*
		Von Hippel-Lindau disease	NCT00970970 (2009)	N.A.; completed	*(3)*
		Primary breast cancer	NCT00991978 (2011)	Phase 1; completed	*(4)*
		Metastatic renal cell carcinoma	NCT01028638 (2011)	N.A.; completed	*(5)*
		Neuroendocrine tumors	NCT01338090 (2011)	N.A.; completed	*(6)*
		Metastatic breast cancer	NCT01081613 (2010)	N.A.; completed	
		Pontine glioma children	NTR3518 (2011)	M.A.; completed	*(7,8)*
		Non-small cell lung cancer		Phase 1; completed	*(9)*
		Inflammatory breast cancer	NCT01894451 (2013)	Phase 1; completed	
		Multiple myeloma	NCT01859234 (2013)	N.A; unknown	
		Pulmonary arterial hypertension	NCT03166306 (2017)	Phase 1,2; recruiting	

Cetuximab	EGFR	Stage IV cancer Adaptive radiation treatment Head and neck cancer Metastatic colorectal cancer Metastatic colorectal cancer	NCT00691548 (2008) NCT01504815 (2012) NCT01691391 (2012) NCT02117466 (2014)	Phase 1; completed Phase 3; completed N.A.; completed Phase 1, 2; completed	*(10)* *(11)* *(12)* *(13)*
Daratumumab	CD38	Multiple myeloma Multiple myeloma	NCT03665155 (2018) NCT04467281 (2020)	Phase 1, 2; completed Phase 2; recruiting	*(14,15)*
Durvalumab	PD-L1	Head and neck cancer Non-small cell lung cancer	NCT03829007 (2019) EudraCT 2019-004284-51	Phase 1,2; recruiting N.A. recruiting	
IbritumumabTiuxitan	CD20	Non-Hodgkins lymphoma		Completed	*(16)*
Ipilumumab	CTLA-4	Melanoma	NCT03313323 (2017)	Phase 2; recruiting	
Nanocolloid albumin (nano-colloid)	Non-targeted	Sentinel lymph node identification Head and neck cancer Sentinel lymph node identification colon cancer	 NCT02850783 (2016)	N.A.; completed Phase 2,3; completed	*(17)* *(18)*
Nimotuzumab	EGFR	Lung and colorectal cancer	NCT04235114 (2020)	Phase 1,2; recruiting	
Nivolumab	PD-1	Non-small cell lung cancer	EudraCT: 2015-004760-11	N.A.; completed	*(19)*
Obinutuzumab	CD20				
Ofatumumab	CD20		EudraCT 2012-001597-29	N.A.; completed	

Panitumumab	EGFR	Metastatic colon cancer	NCT03764137 (2018)	Phase 1,2; recruiting	*(20)*
		Head and neck cancer	NCT03733210 (2018)	N.A.; recruiting	
Pembrolizumab	PD-1	Melanoma, non-small cell lung cancer	NCT02760225 (2016)	N.A.; completed	
		Non-small cell lung cancer	NCT03065764 (2017)	Phase 2; recruiting	
Pertuzumab	HER2	HER2+ carcinoma	NCT03109977 (2017)	Phase 1; completed	*(21)*
Rituximab	CD20	Non-Hodgkin lymphoma: scouting 90Y-ritiximab radioimmunotherapy	EudraCT: 2011-005474-38	N.A.; completed	*(22)*
		Interstitial Pulmonitis	NCT02251964 (2014)	Phase 2,3; completed	*(23)*
		Central nervous system lymphoma	2015-000056-23	N.A.; completed	*(24)*
		Rheumatoid arthritis		N.A.; completed	*(25)*
		Multiple sclerosis		N.A.; completed	*(26)*
		Diffuse large B cell lymphoma	EudraCT 2012-001597-29	N.A.; completed	*(27)*
Trastuzumab	HER2	HER2+ metastatic breast cancer		N.A.; completed	*(28)*
		Metastatic breast cancer	NCT01081600 (2010)	N.A.; completed	*(29)*
		HER2+ metastatic breast cancer	NCT01420146 (2011)	Phase 1; completed	
		HER2+ metastatic breast cancer	NCT01565200 (2012)	Phase 2, completed	*(30)*
		Metastatic breast cancer	NCT01832051 (2013)	Phase 2; completed	*(31)*
		Esophagogastric cancer	NCT02023996 (2013)	N.A.: ongoing, not recruiting	*(32)*
		Metastatic breast cancer	NCT01957332 (2013)	N.A.: ongoing, Not recruiting	
		Metastatic breast cancer	NCT02065609 (2014)	Phase 1; completed	*(33,34)*

		HER2 + breast cancer Breast cancer	NCT02286843 (2014) NCT03321045 (2017)	N.A.; completed Phase 1; recruiting	*(35,36)*

^{89}Zr-non-registered biopharmaceutical	**Target**	**Indication/purpose**	**Trial identified**	**Phase/status**	**References**
ABT-806	EGFRvIII	High grade glioma	NCT03058198 (2017)	N.A.; recruiting	
AMG211 (bispecific)	CD3/CEA	Advanced relapsed/refractory gastrointestinal adenocarcinoma	NCT02760199 (2016)	Phase 1; completed	*(37)*
BI754111	LAG3	Non-small cell lung cancer Head and neck cancer	NCT03780725 (2018)	Phase 1; recruiting	
CER-001 (nanoparticle)	Non-targeted	Atherosclerosis	EudraCT 2014-001666-10	N.A.; completed	*(38)*
CPC634 (Nanoparticle)	Non-targeted	Solid tumors	NCT03712423 (2018)	Phase 1; completed	
cRGDY-PEG-Cy5-C' (Nanoparticle)	Targeted	Malignant brain tumors	NCT03465618 (2018)	Phase 1; recruiting	
DS-8895a	EphA2	Metastatic EphA2+ tumors	NCT02252211 (2014)	Phase 1; completed	
Fresolimumab (GC1008)	TGF-β	Primary brain tumors	NCT01472731 (2011)	Phase 2; completed	*(39)*
Girentuximab	CAIX	Clear cell renal cell carcinoma Renal cell carcinoma	NCT02228954 (2014) NCT02883153 (2016)	N.A.; ongoing, not recruiting Phase 2, 3; completed	*(40)* *(41)*

		Clear cell renal cell carcinoma	NCT03556046 (2018)	Phase 1; completed	
		Clear cell renal cell carcinoma	NCT03849118 (2019)	Phase 3; recruiting	
		Clear cell renal cell carcinoma	NCT04496089 (2020)	Phase 1,2; recruiting	
GSK3128349 (albumin domain binding antibody)	Albumin	Drug delivery	NCT02829307 (2016)	Phase 1; completed	*(42)*
GSK2849330	HER3	HER3+ solid tumors	NCT02345174 (2015)	Phase 1; completed	*(43)*
HER2-Fab-PAS_{200} (Fab fragment)	HER2	Metastatic breast cancer		Pilot	*(44)*
huMab-5B1 (MVT-2163)	CA19.9	Pancreatic cancer Tumors that express CA 19.9	NCT02687230 (2016)	Phase 1; recruiting	
J591	PSMA	Prostate cancer	NCT01543659 (2012)	Phase 1,2; completed	*(45,46)*
		Glioblastoma	NCT02410577 (2015)	N.A.; completed	
		Prostate cancer	NCT02693860 (2016)	Phase 1; completed	
KN035	PD-L1	Advanced solid tumors	NCT03638804 (2018)	N.A.; recruiting	
IAB2M (minibody)	PSMA	Metastatic prostate cancer	NCT01923727 (2013)	Phase 1,2; completed	*(47)*
		Prostate cancer	UMIN000015356 (2014)	Phase 1; completed	*(48)*
		Glioma	UMIN000018639 (2015	Phase 1,2; completed	*(49)*
		Prostate cancer	NCT02349022 (2015)	Phase 2; completed	
		Prostate cancer	NCT03675451 (2018)	Phase 2, completed	
IAB22M2C	CD8	Metastatic solid malignancies,	NCT03107663 (2017)	Phase 1; completed	

		Hodgkin lymphoma Metastatic solid tumors	NCT03802123 (2019)	Phase 2; recruiting	
M7824 (fusion protein)	TGF-β PD-L1	Non-small cell lung cancer	NCT04297748 (2020)	Phase 1, 2: recruiting	
MMOT0530A	Mesothelin	Ovarian, adnexal, digestive system, pancreatic neoplasms/diseases	NCT01832116 (2013)	Phase 1; completed	*(50)*
MSTP2109A	STEAP1	Prostate cancer	NCT01174071 (2013)	Phase 1,2; ongoing, not recruiting	*(51,52)*
REGN3504	PD-L1	Advanced PD-L1 positive malignancies	NCT03746704 (2018)	Phase 1; recruiting	
REGN3767	LAG3	Diffuse large B-cell lymphoma	NCT04566978 (2020)	Phase 1; recruiting	
RO5429083	CD44	Cancer	NCT01358903 (2011)	Phase 1; completed	*(53)*
RO5479599	HER3	HER3+ solid tumors	NCT01482377 (2011)	Phase 1; completed	*(54)*
RO6895882 (immunocytokine)	CEA-ILv2	Cancer	NCT02004106 (2013)	Phase 1; completed	*(55)*
RO7122290 (bi-specific)	FAP 4-1BB (CD137)	Cancer		Recruiting	
TAK-164	Guanylyl Cyclase C	Gastroinstestinal cancer	NCT03449030 (2018)	Phase 1; completed	
SC16.56	DLL3	Small cell lung cancer	NCT04199741 (2019)	Phase 1,2; recruiting	
U36	CD44v6			N.D.; completed	*(56)*

VRC01	HIV-1 envelope	HIV-1 infection	NCT03729752 (2018)	Phase 1; recruiting

* Biopharmeuticals are intact mAbs, except when indicated differently

Data was obtained from the following registries: ClinicalTrials.gov: www.clinicaltrials.gov; EU Clinical Trial Registry: www.clinicaltrialsregistry.eu; UMIN Clinical Trial Registry: www.umin.ac.jp; Netherlands Trial Register: www.trialregister.nl

Abbreviations: CA19.9, carbohydrate antigen 19.9; CAIX, carbonic anhydrase IX; CD3, cluster of differentiation 3; CD8, cluster of differentiation 8; CD20, cluster of differentiation 20; CD38, cluster of differentiation 38; CD44, cluster of differentiation 44; CD44v6, splice variant of CD44 containing variable domain 6; CEA, carcinoembryonic antigen; CTLA-4, cytotoxic T-lymphocyte-associated protein 4; DLL3, delta-like ligand 3; EphA2, ephrin type-A receptor 2; EGFRvIII, epidermal growth factor receptor variant III; FAP, fibroblast activation protein; HER2, human epidermal growth factor receptor 2; HER3, human epidermal growth factor receptor 3; HIV-1, human immunodeficiency virus 1; ILv2, mutated version of interleukin-2; LAG3, lymphocyte-activation gene 3; PD-1, programmed cell death protein 1; PD-L1, programmed death-ligand 1; PSMA, prostate specific membrane antigen; STEAP1, six transmembrane epithelial antigen of prostate 1; TGF-ß, transforming growth factor beta; VEGF, vascular endothelial growth factor.

REFERENCES

1. Bensch F, Van der Veen EL, Lub-de Hooge MN, et al. ^{89}Zr-atezolizumab imaging as a non-invasive approach to assess clinical response to PD-L1 blockade in cancer. *Nat Med.* 2018;24:1852-1858.

2. Oosting SF, Brouwer AH, Van Es SC, et al. ^{89}Zr-bevacizumab PET visualizes heterogeneous tracer accumulation in tumor lesions of renal cell carcinoma patients and differential effects of antiangiogenic treatment. *J Nucl Med.* 2015;56:63-69.

3. Oosting SF, Van Asselt SJ, Brouwers AH, et al. ^{89}Zr-bevacizumab PET visualizes disease manifestations in patients with Von Hippel-Lindau disease. *J Nucl Med.* 2016;57:1244-1250.

4. Gaykema SBM, Brouwers AH, Lub-de Hooge MN, et al. ^{89}Zr-bevacizumab PET imaging in primary breast cancer. *J Nucl Med.* 2013;54:1014-1018.

5. Van Es SC, Brouwers AH, Mahesh SVK, et al. ^{89}Zr-bevacizumab PET: potential early indicator of everolimus efficacy in patients with metastatic renal cell carcinoma. *J Nucl Med.* 2017;58:905-910.

6. Van Asselt SJ, Oosting SF, Brouwers AH, et al. Everolimus reduces ^{89}Zr-bevacizumab tumor uptake in patients with neuroendocrine tumors. *J Nucl Med.* 2014;55:1087-1092.

7. Jansen MH, Veldhuijzen van Zanten SEM, Van Vuurden DG, et al., Molecular drug imaging: ^{89}Zr-bevacizumab PET in children with diffuse intrinsic pontine glioma. *J Nucl Med.* 2017;58:711–716.

8. Veldhuijzen van Zanten SEM, Sewing ACP, Van Lingen A, et al. Multiregional tumor drug-uptake imaging by PET and microvascular morphology in end-stage diffuse intrinsic pontine glioma. *J Nucl Med.* 2018;59:612-615.

9. Bahce I, Huisman MC, Verwer EE, et al. Pilot study of ^{89}Zr-bevacizumab positron emission tomography in patients with advanced non-small cell lung cancer. *EJNMMI Res.* 2014;4:35.

10. Van Loon J, Even AJG, Aerts HJWL, et al. PET imaging of zirconium-89 labelled cetuximab: A phase I trial in patients with head and neck and lung cancer. *Radiother Oncol.* 2017;122:267-273.

11. Even AJG, Hamming-Vrieze O, Van Elmpt W, et al. Quantitative assessment of zirconium-89 labeled cetuximab using PET/CT imaging in patients with advanced head and neck cancer: a theragnostic approach. *Oncotarget.* 2017;8:3870-3880.

12. Menke-van der Houven van Oordt CW, Gootjes EC, Huisman MC, et al. ^{89}Zr-cetuximab PET imaging in patients with advanced colorectal cancer. *Oncotarget.* 2015;6:30384-30393.

13. Van Helden EJ, Elias SG, Gerritse SL, et al. [^{89}Zr]Zr-cetuximab PET/CT as biomarker for cetuximab monotherapy in patients with RAS wild-type advanced colorectal cancer. *Eur J Nucl Med Mol Imaging.* 2020;47:849-859.

14. Ulaner GA, Lyashchenko SK, Riedl C, et al. First-in-human human epidermal growth factor receptor 2-targeted imaging using ^{89}Zr-pertuzumab PET/CT: dosimetry and clinical application in patients with breast cancer. *J Nucl Med.* 2018;59:900-906.

15. Ulaner GA, Sobol NB, O'Donoghue JA, et al. CD38-targeted immuno-PET of multiple myeloma: from xenograft models to first-in-human imaging. *Radiology.* 2020;259:606-615.

16. Rizvi SNF, Visser OJ, Vosjan MJDW, et al. Biodistribution, radiation dosimetry and scouting of ^{90}Y-ibritumomab tiuxetan therapy in patients with relapsed B-cell non-Hodgkin's lymphoma using 89Zr-ibritumomab tiuxitan and PET. *Eur J Nucl Med Mol Imaging.* 2012;39:512-520.

17. Heuveling DA, Van Schie A, Vugts DJ, et al. Pilot study on the feasibility of PET/CT lymphoscintigraphy with ^{89}Zr-nanocolloid albumin for sentinel node identification in oral cancer patients. *J Nucl Med.* 2013;54:585-589.

18. Ankersmit M, Hoekstra OS, Van Lingen A, et al. Perioperative PET/CT lymphoscintigraphy and fluorescent real-time imaging for sentinel node mapping in early staged colon cancer. *Eur J Nucl Med Mol Imaging.* 2019;46:1495-1505.

19. Niemeijer AN, Leung D, Huisman MC, et al. Whole body PD-1 and PD-L1 positron emission tomography in patients with non-small-cell lung cancer. *Nat Commun.* 2018;9:4664.

20. Lindenberg L, Adler S, Turkbey IB, et al. Dosimetry and first human experience with ^{89}Zr-panitumumab. *Am J Nucl Med Mol Imaging.* 2017;7:195-203.

21. Ulaner GA, Carrasquillo JA, Riedl CC, et al. Identification of HER2-positive metastases in patients with HER2-negative primary breast cancer by using HER2-targeted ^{89}Zr-Pertuzumab PET/CT. *Radiology* 2020;296:370-378.

22. Muylle K, Flamen P, Vugts DJ, et al. Tumour targeting and radiation dose of radioimmunotherapy with ^{90}Y-rituximab in CD20+ B-cell lymphoma as predicted by ^{89}Zr-rituximab immuno-PET: impact of preloading with unlabelled rituximab. *Eur J Nucl Med Mol Imaging.* 2015;42:1304-1314.

23. Adams H, Van de Garde EMW, Van Moorsel CHM, et al. [^{89}Zr]Zr-rituximab PET/CT activity in patients with therapy refractory interstitial pneumonitis: a feasibility study. *Am J Nucl Med Mol Imaging.* 2019;9:296-308.

24. Laban KG, Kalmann R, Leguit RJ, De Keizer B. Zirconium-89-labelled rituximab PET-CT in orbital inflammatory disease. *EJNMMI Res.* 2019;9:69.

25. Bruijnen S, Tsang-A-Sjoe M, Raterman H, et al. B-cell imaging with zirconium-89 labelled rituximab PET/CT at baseline is associated with therapeutic response 24 weeks after

initiation of rituximab treatment in rheumatoid arthritis patients. *Arthritis Res Ther.* 2016;18:266.

26. Hagens MHJ, Killestein J, Yaqub MM et al. Cerebral rituximab uptake in multiple sclerosis: A ^{89}Zr-immunoPET pilot study. *Mult Scler.* 2018;24:543-545.

27. Jauw YWS, Zijlstra JM, De Jong D, et al. Performance of ^{89}Zr-labeled-rituximab-PET as an imaging biomarker to assess CD20 targeting: A pilot study in patients with relapsed/refractory diffuse large B cell lymphoma. *PLOS One.* 2017;12:e0169828.

28. Dijkers EC, Oude Munnink TH, Kosterink JG, et al. Biodistribition of ^{89}Zr-trastuzumab and PET imaging of HER2-positive lesions in patients with metastatic breast cancer. *Clin Pharmacol Ther.* 2010;87:586-592.

29. Gaykema SBM, Schröder CP, Vitfell-Rasmussen J, et al. ^{89}Zr-trastuzumab and ^{89}Zr-bevacizumab PET to evaluate the effect of the HSP90 inhibitor NVP-AUY922 in metastatic breast cancer patients. *Clin Cancer Res.* 2014;20:3945-3954.

30. Gebhart G, Lamberts LE, Wimana Z, et al. Molecular imaging as a tool to investigate heterogeneity of advanced HER2-positive breast cancer and to predict patient outcome under trastuzumab emtansine (T-DM1): the ZEPHIR trial. *Ann Oncol.* 2016;27:619-624.

31. Bensch F, Brouwers AH, Lub-de Hooge MN, et al. ^{89}Zr-trastuzumab PET supports clinical decision making in breast cancer patients, when HER2 status cannot be determined by standard work up. *Eur J Nucl Med Mol Imaging.* 2018;45:2300-2306.

32. O'Donoghue JA, Lewis JS, Pandit-Taskar N, et al. Pharmacokinetics, biodistribution, and radiation dosimetry for ^{89}Zr-trastuzumab in patients with esophagogastric cancer. *J Nucl Med.* 2018;59:161-166.

33. Dehdashti F, Wu N, Bose R, et al. Evaluation of [^{89}Zr]trastuzumab-PET/CT in differentiating HER2-positive from HER2-negative breast cancer. *Breast Cancer Res Treat* 2018;169:523-530.

34. Laforest R, Lapi SE, Oyama R, et al. [^{89}Zr]Trastuzumab: evaluation of radiation dosimetry, safety, and optimal imaging parameters in women with HER2-positive breast cancer. *Mol Imaging Biol.* 2016;18:952-959.

35. Ulaner GA, Hyman DM, Ross DS, et al. Detection of HER2-positive metastases in patients with HER2-negative primary breast cancer using ^{89}Zr-trastuzumab PET/CT. *J Nucl Med.* 2016;57:1523-1528.

36. Ulaner GA, Hyman DM, Lyashchenko SK, et al. ^{89}Zr-trastuzumab PET/CT for detection of HER2-positive metastases in patients with HER2-negative primary breast cancer. *Clin Med Nucl.* 2017;42:912-917.

37. Moek KL, Waaijer SJH, Kok IC, et al. ^{89}Zr-labeled bispecific T-cell engager AMG 211 PET shows AMG 211 accumulation in CD3-rich tissues and clear, heterogeneous tumor uptake. *Clin Cancer Res.* 2019;25:3517-3527.

38. Zheng KH, Van der Valk FM, Smits LP, et al. HDL mimetic CER-001 targets atherosclerotic plaques in patients. *Atherosclerosis.* 2016;251:381-388.

39. Den Hollander MW, Bensch F, Glaudemans AWJM, et al. TGF-β antibody uptake in recurrent high-grade glioma imaged with ^{89}Zr-fresolimumab PET. *J Nucl Med.* 2015;56:1310-1314.

40. Verhoeff SR, Van Es SC, Boon E, et al. Lesion detection by [^{89}Zr]Zr-girentuximab and [^{18}F]FDG-PET/CT in patients with newly diagnosed metastatic renal cell carcinoma. *Eur J Nucl Med Mol Imaging.* 2019;16:1931-1939.

41. Hekman MCH, Rijpkema M, Aarntzen EH, et al. Positron emission tomography/computed tomography with ^{89}Zr-girentuximab can aid in diagnostic dilemmas of clear cell carcinoma suspicion. *Eur Urol.* 2018;74:257-260.

42. Thorneloe KS, Sepp A, Zhang S, et al. The biodistribution and clearance of AlbudAb, a novel biopharmaceutical medicine platform, assessed via PET imaging in humans. *EJNMMI Res.* 2019;9:45.

43. Menke-van der Houven van Oordt CW, McGeoch A, Bergstrom M, et al. Immuno-PET imaging to assess target engagement: experience from ^{89}Zr-anti-HER3 mAb (GSK2849330) in patients with solid tumors. *J Nucl Med.* 2019;60:902-909.

44. Richter A, Knorr K, Schlapschy M, et al. First-in-human medical imaging with PASylated ^{89}Zr-labeled anti-HER2 Fab-fragment in a patient with metastatic breast cancer. *Eur J Nucl Med Mol Imaging.* 2020;54:114-119.

45. Pandit-Taskar N, O'Donoghue JA, Durack JC, et al. A phase I/II study for analytic validation of ^{89}Zr-J592 immunoPET as a molecular imaging agent for metastatic prostate cancer. *Clin Cancer Res.* 2015;21:5277-5285.

46. Pandit-Taskar N, O'Donoghue JA, Beylergil V, et al. ^{89}Zr-huJ592 immuno-PET imaging in patients with advanced metastatic prostate cancer. *Eur J Nucl Med Mol Imaging.* 2014;41:2093-2105.

47. Pandit-Taskar N, O'Donoghue JA, Ruan S, et al. First-in-human imaging with ^{89}Zr-Df-IAB2M anti-PSMA minibody in patients with metastatic prostate cancer: pharmacokinetics, biodistribution, dosimetry and lesion uptake. *J Nucl Med.* 2016;57:1858-1864.

48. Joraku A, Hatano K, Kawai K, et al. Phase I/II PET imaging study with ^{89}zirconium labeled anti-PSMA minibody for urological malignancies. *Ann Nucl Med.* 2019;33:119-127.

49. Matsuda M, Ishikawa E, Yamamoto T, et al. Potential use of prostate specific membrane antigen (PSMA) for detecting the tumor neovasculature of brain tumors by PET imaging with ^{89}Zr-Df-IAB2M anti-PSMA minibody. *J Neurooncol.* 2018;138:581-589.

50. Lamberts LA, Menke-van der Houven van Oordt CW, Ter Weede EJ, et al. ImmunoPET with anti-mesothelin antibody in patients with pancreatic and ovarian cancer before anti-mesothelin antibody-drug conjugate treatment. *Clin Cancer Res.* 2016;22:1642-1652.

51. Carrasquillo JA, Fine BM, Pandit-Taskar N, et al. Imaging patients with metastatic castration-resistant prostate cancer using ^{89}Zr-DFO-MSTP2109A anti-STEAP1 antibody. *J Nucl Med.* 2019;60:1517-1523.

52. O'Donoghue, Danila DC, Pandit-Taskar N, et al. Pharmacokinetics and biodistribution of a [^{89}Zr]Zr-DFO-MSTP2109A anti-STEAP antibody in metastatic castration-resistant prostate cancer patients. *Mol Pharm.* 2019;16:3083-3090.

53. Menke-van der Houven van Oordt CW, Gomez-Roca C, Van Herpen C, et al. First-in-human phase I clinical trial of RG7356, an anti-CD44 humanized antibody, in patients with advanced, CD44-expressing solid tumors. *Oncotarget.* 2016;7;80046-80058.

54. Bensch F, Lamberts LE, Smeenk MM, et al. ^{89}Zr-Lumretuzumab PET imaging before and during HER3 antibody lumretuzumab treatment is patients with solid tumors. *Clin Cancer Res.* 2017;23:6128-6137.

55. Van Brummelen EMJ, Huisman MC, De Wit-Van der Veen LJ, et al. ^{89}Zr-labeled CEA-targeted IL-2 variant immunocytokine in patients with solid tumors: CEA-mediated tumor accumulation and role of IL-2 receptor binding. *Oncotarget.* 2018;9:24737-24749.

56. Börjesson PKE, Jauw YWS, Boellaard R, et al. Performance of immuno-positron emission tomography with zirconium-89-labeled chimeric monoclonal antibody U36 in the detection of lymph node metastases in head and neck cancer patients. *Clin Cancer Res.* 2006;12:2133-2140.